



Soft Matter

Tunable Assembly of Host–Guest Colloidal Crystals

Journal:	<i>Soft Matter</i>
Manuscript ID	SM-ART-07-2023-000891.R1
Article Type:	Paper
Date Submitted by the Author:	23-Aug-2023
Complete List of Authors:	Dwyer, Tobias; University of Michigan College of Engineering, Chemical Engineering Moore, Timothy; University of Michigan, Chemical Engineering Anderson, Joshua; University of Michigan, Chemical Engineering Glotzer, Sharon; University of Michigan, Chemical Engineering

SCHOLARONE™
Manuscripts

Cite this: DOI: 00.0000/xxxxxxxxxx

Tunable Assembly of Host–Guest Colloidal Crystals[†]

Tobias Dwyer,^a Timothy C. Moore,^a Joshua A. Anderson,^b and Sharon C. Glotzer^{ab*}

Received Date

Accepted Date

DOI: 00.0000/xxxxxxxxxx

Entropy compartmentalization provides new self-assembly routes to colloidal host–guest (HG) structures. Leveraging host particle shape to drive the assembly of HG structures has only recently been proposed and demonstrated. However, the extent to which the guest particles can dictate the structure of the porous network of host particles has not been explored. In this work, by modifying only the guest shape, we show athermal, binary mixtures of star-shaped host particles and convex polygon-shaped guest particles assemble as many as five distinct crystal structures, including rotator and discrete rotator guest crystals, two homoporous host crystals, and one heteroporous host crystal. Edge-to-edge alignment of neighboring stars results in the formation of three distinct pore motifs, whose preferential formation is controlled by the size and shape of the guest particles. Finally, we confirm, via free volume calculations, that assembly is driven by entropy compartmentalization, where the hosts and guests contribute differently to the free energy of the system; free volume calculations also explain differences in assembly based on guest shape. These results provide guest design rules for assembling colloidal HG structures, especially on surfaces and interfaces.

1 Introduction

Hard, anisotropic particles assemble into a rich variety of crystalline structures, both with and without corresponding atomic analogs.^{1–6} Because there are no energetic interactions between particles in such systems, entropy maximization drives their self-assembly and thermodynamic stability.^{7–11} At moderate density, systems of convex particles assemble into locally dense structures that minimize local excluded volume, which generally promotes the face-to-face alignment of particles to optimize local entropic bonding and maximize system entropy.^{2,11} Consequently, the entropy-driven assembly of open structures in the absence of enthalpic interactions is unusual.^{2,3} However, open structures with well-defined, regularly arranged pores have many potential applications, and are therefore sought after in the nanoparticle and colloidal self-assembly communities. For example, many photonic crystals are open structures,^{12–15} and open structures display interesting structural^{16–18} and phononic properties,^{19–22} as well as the ability to adsorb particles into their pores.^{23–25} Open structures are therefore an important target in the development of functional nanoparticle systems.

Concave shapes may offer an alternative route to shape-driven

self-assembly of open structures because some concave shapes can form structures that are locally dense but still contain regularly arranged voids between particles. Few such structures have been reported in the literature, but a growing body of work has shown the potential for concave particles to form porous assemblies. One example is the porous structures formed by star-shaped particles both with and without interparticle attraction.^{26,27} Multicomponent systems offer another promising route to the assembly of open structures following the removal of one component.²⁸ Although self-assembly in binary hard sphere systems is well-studied,^{6,29,30} multicomponent systems of hard, anisotropic particles are relatively underexplored in the literature, with only a few examples of substitutionally ordered lattices (co-crystals) reported. The existing literature on co-crystals of aspherical hard particles includes binary assemblies of tetrahedra and octahedra,³ shape allophiles that assemble a square lattice,³¹ octapod–sphere assemblies,⁵ hard polyhedron crystals isostructural to clathrate hydrates,³² and notched triangle–rectangle host–guest (HG) structures.³³

The notched triangle systems are binary, athermal systems comprising concave “notched” triangle host particles and rectangular guest particles where the hosts form an open network structure. The hosts form a honeycomb lattice with a single pore shape (i.e., a homoporous network), with rectangles freely rotating within the pores of the structure. We denote these as open structures because the host particles occupy only 30–35% of the area of the system. While the notched triangle system showed that HG assembly is possible in athermal systems, several questions remain: (i) Can simpler, readily synthesizable concave shapes assemble

^a Department of Chemical Engineering, University of Michigan, Ann Arbor, MI, USA.

^b Biointerfaces Institute, University of Michigan, Ann Arbor, MI, USA.

[†] Electronic Supplementary Information (ESI) available: Animation of simulations with each guest shape; Host and guest body orientation distributions, hexatic order parameter distributions, and body orientation correlation functions; Schematic showing that shield pore hexamers cannot tile space alone. See DOI: 10.1039/cXsm00000x/

homoporous HG structures? (ii) Can the shape of the guest particles control the pore morphology of the host structure (i.e., to selectively assemble homoporous or heteroporous structures)? (iii) Is the entropy compartmentalized in these systems? Recently published simulations show that self-assembled hard polyhedron clathrates "compartmentalize" the entropy into subsystems of relatively immobile hosts and highly mobile guests. In this work we answer all of these questions in the affirmative and highlight the implications of entropy compartmentalization for colloidal HG self-assembly.

The remainder of this paper proceeds as follows: we first show that mixtures of 3-pointed star-shaped host particles and either square or small-hexagon guest particles form heteroporous HG crystals isostructural to those observed in systems of attractive star-shaped particles²⁶. We then show that the structure of the porous network of host particles depends on the size and shape of the guest particles, such that one can use the guest particles to tune the structure of the host particle network. Finally, we show that entropy is compartmentalized in these HG systems using free volume calculations. We show guest-pore shape complementarity and guest particle size determine the degree of entropy compartmentalization, indicating a means to tune entropy compartmentalization in these systems.

2 Model and Methods

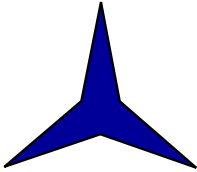

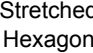

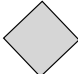
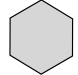
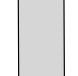
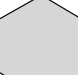

Star Host Particle	Guest Shape	Pores
 Observed Pore Motifs  Hexagon  Stretched Hexagon  Shield		Stretched, Hexagon, and Shield Fig. 2a
		Stretched, Hexagon, and Shield Fig. 2d
		Stretched Fig. 4a
		Hexagon Fig. 4d
		Hexagon and Shield Fig. 4g

Fig. 1 Top left: star particle used in this work (not to scale with guests). Bottom left: three possible arrangements of star particles to make a pore, including the "hexagon," "stretched hexagon," and "shield" pore shapes. Right: table of convex guest particles simulated in this study, labeled by pores observed in each structure.

We performed 2D hard particle Monte Carlo (HPMC) simulations with HOOMD-Blue version 3.5.0.^{34,35} All systems contain a single concave host particle type (a star) and one of 5 convex guest particle types, shown in Fig. 1. We define the star particles by a single parameter, the spoke ratio R_S , which is the ratio of

the incircle radius R_i to the circumcircle radius R_c of the particle. $R_S = 0.5$ defines a regular triangle, and $R_S < 0.5$ characterizes concave particles. The radius of the host particle's circumcircle defines the length unit σ used in this work, with $\sigma = R_c/2$ (σ is also the incircle radius of a star particle when $R_S = 0.5$). All systems contain star particles with $R_S = 0.2$. Depending on the guest particle size and shape, the star particles can form different pore motifs, as summarized in Fig. 1.

For the guest particles in the heteroporous assembly simulations, we chose a square with an edge length $\approx 2.09\sigma$ and a hexagon with the same circumcircle radius, which are both small enough to fit in all of the pore motifs. For the designed assemblies, we used a hexagon with edge length equal to that of the host star edge length to promote hexagon pores. To promote stretched pores, we used a rectangle with dimensions $3.6\sigma \times 1.8\sigma$, which cannot fit in the hexagon pores at high density. To promote neither hexagon nor stretched pores, we used a shield-shaped guest with edge length equal to the star particle edge length.

We initialized all assembly simulations with 2000 host particles and 1000 guest particles in demixed configurations at an area fraction $\phi = 0.45$ in a 2D square box with periodic boundary conditions and allowed the systems to mix over $5e6$ steps at constant density. We then started isobaric simulations where we slowly compressed the system over 10 million timesteps from an initial pressure ($P^* = \beta P \sigma^2 = 1$) to the target pressure where (assembly conditions varied based on size and shape). In the figures shown in this work, the assembly pressures for each shape were $P^* = 3$ (squares, rectangles), $P^* = 2.5$ (small-hexagons, large-hexagons, shields). We ran the simulations for 140 million HPMC steps (except for the rectangles, which required 300 million steps for assembly) at the final pressure. In our simulations, box volume moves as well as displacement and rotations of particles were tuned to have an acceptance rate of 33%. We confirmed equilibration of each system by ensuring the density and diffraction pattern reached a steady state after assembly at constant P^* . We show mixing and constant P^* simulations for each shape in the Supplementary Information.

To differentiate the guest rotator from the crystal and discrete rotator phases we analyzed the body orientation of the guest particles, distributed from $(-\pi/n, \pi/n)$, where n is the order of rotational symmetry of the guest particle (hexagon ($n = 6$), square (4), rectangle (2)), except in the case of shield-shaped guests where we use $n = 6$ to account for the symmetry of shield-shaped pores in an extended porous network. To detect systems with hexagon pores we calculated the hexatic bond orientational order of the host particles as

$$\psi_j = \frac{1}{N} \left| \sum_{k=1}^N e^{6i\theta_{k,j}} \right|,$$

where N is the number neighbors within the first peak of the host-host radial distribution, where $\theta_{k,j}$ is the angle between the vector connecting the centroid of host particle k to host particle j and an arbitrary reference vector, and $\psi_j = 1$ indicates perfect local hexatic ordering.

To examine the different entropic contributions to the stabil-

ity of the HG structures, we performed Monte Carlo integration to estimate the free volume available to host and guest particles in different pore configurations. The free volume of particles in a structure serves as a way to estimate the configurational volume available to each particle and thereby the relative entropic contributions of each type of particle in the system. Following the method of Qi *et al.*³⁶, we considered a single unit cell of the structure and worked under a mean field approximation (MFA) where we held all but one particle (the “test particle”) stationary. We then rotated the test particle through a full rotation in the plane in increments of $2\pi/100$. At each orientation, we performed $\approx 66,666$ trial insertions where we placed the particle at a random position within the unit cell and checked for overlaps with the stationary particles. The fraction of configurations with zero particle overlaps multiplied by the area of the test system gives the free volume (here, free area) of the test particle $A_f(\theta)$ as a function of the orientation of the test particle θ . Integration of $A_f(\theta)$ over all orientations gives the total free volume available to the particle within the unit cell \bar{A}_f :

$$\bar{A}_f = (2\pi)^{-1} \int_{-\pi}^{\pi} A_f(\theta) d\theta.$$

We repeated the calculation over 5 replicas and obtain a maximum standard error of the means of less than two percent in free volume for each particle type for all systems studied. We defined the degree of entropy compartmentalization ξ as the ratio of the free volume of the guest and host particles, $\xi = \bar{A}_{f,\text{guest}}/\bar{A}_{f,\text{host}}$. A value of ξ much greater or less than 1 indicates significant entropy compartmentalization. To estimate the free energy difference between pore types, we computed the free energy under a MFA where the free volumes of the particles in the unit cell are assumed to be uncorrelated. The intensive Helmholtz free energy of the system can be written as³⁷:

$$f = \frac{F}{Nk_B T} = -\langle \ln(\bar{A}_f) \rangle.$$

Data and workflow management for this project was supported by the *signac* data management framework.³⁸ We used *freud*³⁹ and *NumPy*⁴⁰ for data analysis, all plots were generated via *Matplotlib*,⁴¹ and we used *coxeter*⁴² to calculate shape information (e.g. the area of the star particles). Visualizations of the systems were generated using *Ovito*.⁴³ Assembly simulations were conducted using *HOOMD-blue* v3.5.0³⁴ using XSEDE resources.⁴⁴

3 Results

3.1 Assembly of Heteroporous, Rotator HG Crystals

Figures 2a,d show the final snapshots from simulations of systems self-assembled with square and small-hexagon guests, respectively. In both systems, the star particles form pores around the guest particles, becoming orientationally restrained in the process (see body orientation distributions, and orientation correlation functions in Fig. S1). Visually, the systems appear highly ordered, and the diffraction patterns in the insets of Fig. 2b,c,e,f indicate crystalline-like order in the systems. Visual inspection reveals that the structures are heteroporous, containing a mixture of all three

pore shapes highlighted in Fig. 1. We observe the hexagon pore, where all six hexamers make up the pore interior, the stretched pore, where 4 of the 6 stars make up the interior of the pore, and the shield pore, where only 3 of the 6 stars in a hexamer make up the pore interior. The variability in ψ_j also highlights the heteroporosity of the structures. The square-guest system (Fig. 2a-c) contains only small regions of high hexatic order ψ_j (dark regions in Fig. 2b), indicating no large contiguous regions of hexagon pores. The small-hexagon guest system (Fig. 2d-f), in contrast, contains larger regions of high ψ_j , indicating more and larger, continuous regions of hexagonal pores in the system compared to the square-guest system.

The ordering of the guest particles differs between the two systems. The square guests are completely orientationally disordered, as shown visually by their body orientations (Fig. 2c) and quantitatively by the distribution of their orientations (Fig. S1b), and lack of orientational correlation past their first neighbor shell (Fig. S1b). The hexagon guests are relatively more orientationally correlated, but are still able to access all orientational states (Fig. 2f, orientation distribution, and correlation functions in S1a), indicating a discrete rotator phase⁴⁵. Such discrete (continuous) rotator phases were also observed in clathrate HG systems where guest particles matched (did not match) the pore symmetry and guests were smaller than the pore geometries.³²

Notably, we did not observe phase separation or amorphous aggregates of host and guest particles in any simulations, which is often observed in binary systems of hard particles^{46,47}. Instead, all HG structures we observed formed readily and reproducibly, indicating these systems strongly favor mixing and the formation of HG structures. However, neither system formed a homoporous crystal, with the hexagon guest only favoring hexagon pores (the thermodynamic underpinnings of which we investigate in section 3.3). Previous work demonstrated the assembly of a homoporous hexagon pore crystal in systems of edge-attractive stars with repulsive ligands grafted to each vertex that serve to disfavor the tip-tip coordination that is present in the stretched hexagon and shield pores²⁶. However, a particle morphology disfavoring tip-tip proximity only promotes hexagon pores (similar to how previous work on notched triangles³³ allowed for only hexagon pores to form) because the stretched hexagon and shield pores have tip-tip alignment (see Fig. 1).

In this section, we have shown that the shape of the guest particle can promote the formation of one pore shape over another. However, the assemblies of star particles with either small-square or small-hexagon guests, both of which easily fit into any of the possible pore motifs, each contain heteroporous host networks. The following section shows the flexibility of this HG approach to design guests that direct the assembly of homoporous structures (stretched or hexagon).

3.2 Guest Shape Design for Assembly of HG Crystals

The guest particles clearly influence the behavior of the system, as the star particles do not form porous networks in their absence (see Fig. S2). Moreover, the difference in the spatial correlations in pore shapes between systems with small-square and small-hexagon

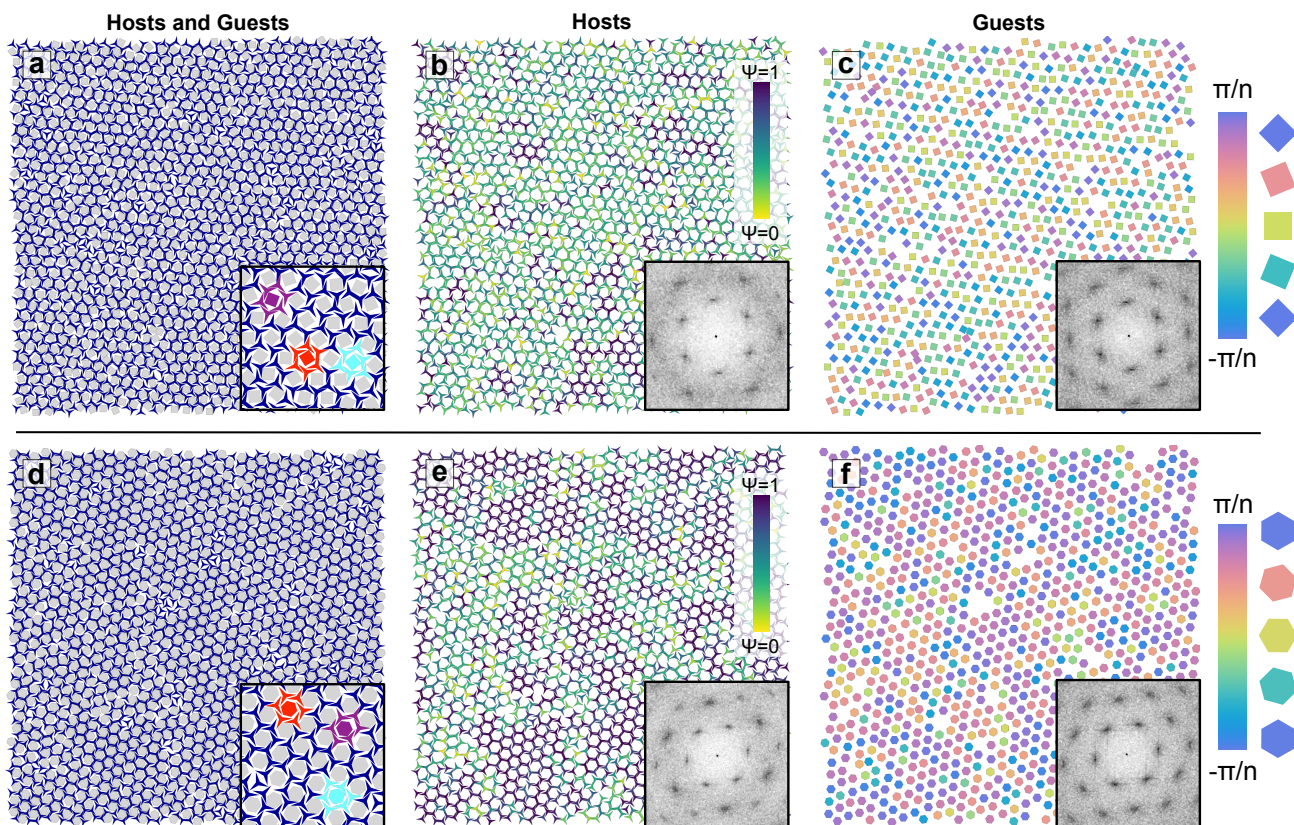


Fig. 2 Final snapshots of self-assembled systems with square guests (a-c) and small-hexagon guests (d-f). a,d: snapshots showing the final self-assembled structures, where particles are colored by their shape (host particles blue, guest particles gray). Insets show a small portion of the system to highlight the different shapes of pores that formed. Selected pores are colored by their shape, consistent with the coloring in Fig. 1. b,e: System snapshots showing only host particles, colored by their hexatic bond-orientational order parameter ψ_j . Contiguous regions of high ψ_j , which are especially apparent in e, indicate regions of predominately hexagon pores. Insets show the diffraction pattern of the host particle positions, whose sharp peaks indicate crystalline order in these systems. c,f: System snapshots showing only guest particles, colored by their body orientation as shown by the reference particles orientations to the right of each row. The presence of all colors in both c and f shows that both guest shapes can explore all orientational configuration space in these systems, consistent with the presence of (discrete) rotator phases.

guests indicate that the shape of the guests has an impact on the structure of the porous host network. The question remains, however, how much control over the assemblies the guests provide, e.g., whether particular guest sizes and shapes can selectively direct the assembly of homoporous versus heteroporous networks. To answer this question, we studied HG systems with three different guest shapes: a rectangle, a regular hexagon, and an equilateral hexagon with D_3 symmetry (which we refer to as a shield-shaped guest particle, see Fig. 3, middle row). We chose the guest sizes such that each guest would fit into only one of the pore shapes, as summarized in Fig. 3.

For the large hexagon guest, we made the size to precisely complement the shape of the hexagon pore by making the guest edge length equal to the edge length of the star. This makes the large hexagon circumcircle larger than the incircle of the stretched or shield pore, thereby geometrically excluding both (Fig. 3). We used the same strategy for the shield guest–pore combination, making the shield guest edge length equal to the star edge length, thereby excluding the hexagon and stretched pores instead (Fig. 3). However, because shield pores cannot tile space (see Fig. S3), we instead expect heteroporous HG structure. This shape complementarity design principle suggests a rectangular guest particle would direct the assembly of stretched pores; we therefore chose a rectangle with a long edge slightly longer than the incircle of a hexagon pore (which excludes hexagon and shield pores) and short edge length slightly less than the edge of a star (to not exclude the stretched pores).

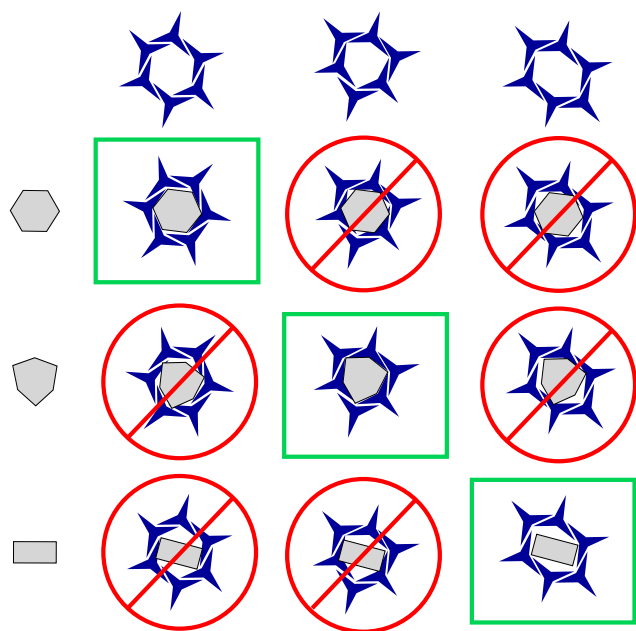


Fig. 3 Summary of proposed design rules for guest-controlled pore morphology in HG systems. Each row corresponds to the single guest shape shown to the left of the row, and each column corresponds to the pore shape shown at the top of the column. Green boxes indicate allowed guest–pore combinations, where the guest fits inside the pore, and red circles indicate geometrically forbidden guest–pore combinations, where the guest does not fit into the pore.

Our self-assembly simulations support these simple design rules,

successfully assembling homoporous crystals with large hexagon and rectangle guests and a heteroporous structure with the shield-shaped guests. For both the large hexagon- and rectangle-guest assemblies, we see the preferential formation of a single pore type (Fig. 4a,d). The hosts surrounding the hexagon guests form mostly hexagon pores, as indicated visually and by the high hexatic order parameter of the host particles ($\langle \psi_j \rangle = 0.77$, see Fig. 4e). Additionally, the hexagon guests are orientationally ordered compared to squares or small-hexagons in Fig. 2c,f, indicating the guests form a crystal rather than a (discrete) rotator crystal. For the rectangle-guest systems, we observe a homoporous crystal of stretched pores. The large regions of nearly constant ψ_j indicate a single pore type, while the lack of regions of high ψ_j are consistent with a lack of hexagon pores. The rectangle guests are also strongly orientationally ordered, forming large grains with a single body orientation (Fig. 4c) and high positional order (as indicated by diffraction pattern insets).

The final test of our design hypothesis used shield-shaped guests, which should favor the formation of shield pores. This test also serves as a qualitative test of the driving force for the formation of HG structures in general for shield guests, as the hosts cannot form an extended network containing only shield pores (see Fig. S3), and the system is therefore inherently frustrated. As a result of this frustration, this system forms a heteroporous crystal (Fig. 4g) where both hexagon and shield pores are present, as indicated by low ψ_j (Fig. 4h, $\langle \psi_j \rangle = 0.46$) in combination with a lack of visually apparent stretched pores. Despite not having a homoporous crystal structure, the system still has long range positional order (as indicated by peaks in the diffraction pattern insets) and orientational order for the host and guests (distributions and correlation functions in Fig. S1e). Even with frustration designed into the HG combination, we still see the formation of a HG crystal, emphasizing the strong driving force for the formation of HG structures. These results show that the guest shape provides a means to control the overall structure in these systems and provides design rules for selecting the uniformity of the pores in general (e.g., homo- versus heteroporous host networks) or the shape of pores in a homoporous network (e.g., hexagon versus stretched hexagon pores).

3.3 Entropic Contributions to Host-Guest Structures

In this section, we investigate the influence of the size and shape of the guest particles relative to the pores on entropy compartmentalization in these systems. Entropy is a system-level (global) thermodynamic quantity. In these HG structures, where the hosts form a relatively rigid network within which the guests rotate, it is reasonable to consider the system comprised of two subsystems, each of which contribute to the total entropy of the system, following previous work³². We decomposed the systems into host and guest subsystems and analyzed the free volume within the HG structures of each species separately. For the analysis, we focused on unit cells of homoporous systems (stretched and hexagon pores) at the same packing fractions ϕ where we observed self-assembly ($\phi = 0.648$, small-hexagons; $\phi = 0.583$, square; $\phi = 0.63$, rectangle; $\phi = 0.737$, large hexagon). Since the shield pores cannot form a

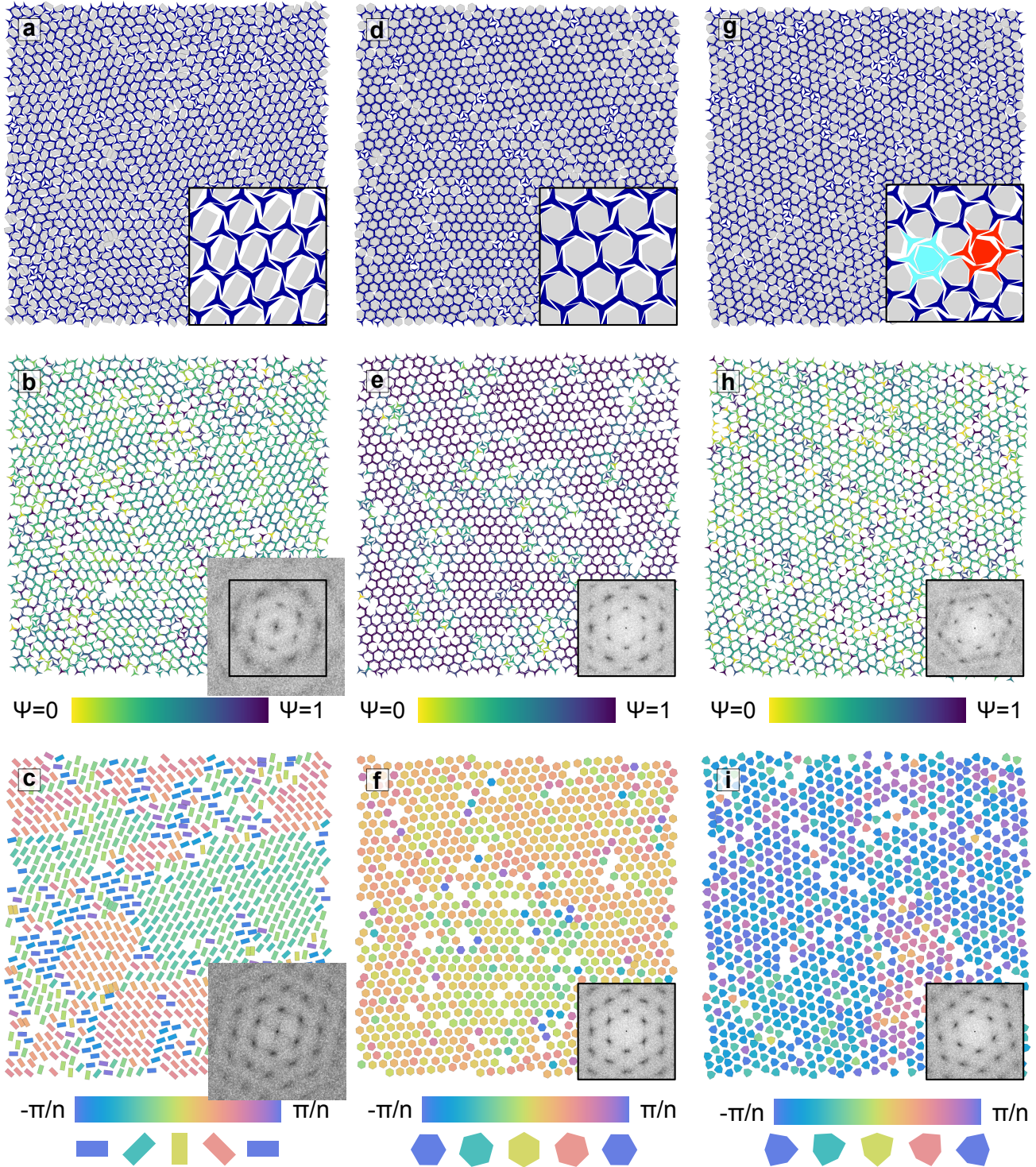


Fig. 4 Influence of guest particle shape on HG self-assembly. Snapshots show systems with rectangular guest particles (a–c), large hexagonal guest particles (d–f), and shield-shaped guest particles (g–i). a,d,g: system snapshots colored the same as Fig. 2a,d. Insets show small subsets of each system, and selected pores in g are colored consistently with Fig. 1. b,e,h: system snapshots showing only the host particles, colored by their hexatic bond-orientational order parameter ψ_j . Contiguous regions of similar color indicate regions of similarly shaped pores, which are apparent in b and e but less prominent in h, consistent with the formation of homoporous (heteroporous) host structures in the presence of rectangular and hexagonal (shield-shaped) guests. Insets show diffraction patterns of the host particle positions, whose bright peaks indicate crystalline order in all systems. c,f,i: system snapshots showing only the guest particles, colored by their body orientation as indicated by the reference particles below each column. The large regions of low variability in color are consistent with orientational order of the guest particles. Insets show the diffraction patterns of the guest particle positions, whose sharp peaks are consistent with crystalline order of the guest particles.

unit cell that tiles space (Fig. S3), we excluded them from the analysis. In each HG structure, the hosts have little orientational freedom, as shown in Fig. S1. For the assemblies with square and small-hexagon guests (Fig. 2), the guest particles have little orientational confinement. In contrast, the guests are orientationally restrained in the self-assembled systems with large hexagon, shield, and rectangular guest particles. Based on these observations, we hypothesize that the greater difference in orientational freedom between host and guest particles for the square and small-hexagon systems versus the rectangle and large hexagon systems indicates a greater degree of entropy compartmentalization.

To decompose the systems into host and guest subsystems, we analyzed the systems within a mean field approximation (MFA). Under the MFA, each particle in the unit cell is caged by its neighboring particles, which are assumed to have a constant orientation and position. We take this as a reasonable assumption because the hosts are orientationally restricted through a combination of edge-edge alignment with neighboring hosts and the guest particle at the center of each pore preventing the hosts from accessing free volume in the pore center. The guest particles are surrounded by hosts, which are orientationally restrained, allowing each guest to only access the free volume of a single pore. Given the athermal nature of these systems, the entropy (and therefore the free energy) of each species is directly proportional to the logarithm of the free volume available to it. We thereby compute the free volume associated with each species and in turn estimate the entropy contributions of host and guest subsystems to the total system entropy.

For the large-hexagon-guest system (Fig. 5a), we see the least entropy compartmentalization, with $\xi \approx 4.1$. The rectangle-guest system (Fig. 5a) also has relatively little entropy compartmentalization ($\xi \approx 8.2$) in the stretched pore, as expected from the orientational distribution functions of the host and guest particles (Fig. S1). The small-hexagon guests, which are shape complementary to the hexagon pores, show slightly higher compartmentalization for both hexagon ($\xi \approx 12.0$) and stretched pores ($\xi \approx 9.6$). Comparison of the large and small hexagon guest systems shows that entropy compartmentalization increases with decreasing guest size due to increased free volume of the smaller guest particles. The entropy compartmentalization is highest when the guest shape does not match the shape of the pores. For square guests, which have the same circumcircle radius as small-hexagon guests, $\xi \approx 17.3(32.3)$ for hexagon (stretched) pores. As in previous work on 3D convex particles³², for shapes of the same size, entropy compartmentalization increases with increasing symmetry mismatch between the shape of the guest particles and the shape of the pores. These calculations show that guest-pore shape complementarity can also be used in 2D HG systems to tune HG entropy contributions.

In addition to estimating entropy compartmentalization, free volume calculations allow us to rationalize two key aspects of HG assembly for square vs small-hexagon guest particles: (1) the formation of a rotator versus a discrete rotator and (2) the higher prevalence of hexagon pores for small-hexagon guests vs square guests. Fig. 5c shows overlap in the peaks of the orientation-dependent free volumes available to small-hexagon guest particles

($A_{f,G}(\theta)$) in the different pore shapes. Due to this overlap, in a self-assembled structure where a low thermodynamic driving force between pore types results in a heteroporous host network, we still expect the guest particles to have strongly localized orientations, resulting in the discrete rotator guest phase we observed in Fig. 2b,f. Conversely, Fig. 5d shows misaligned peaks in $A_{f,guest}(\theta)$ for square guests. When averaged, the two $A_{f,guest}(\theta)$ curves for square guests (gray lines in Fig. 5d) result in a relatively flat $A_{f,guest}(\theta)$, and hence the guest rotator crystal observed in Fig. 2a,g.

Our calculations also help rationalize why the small-hexagon-guest systems form more hexagon pores compared to the square-guest systems and why we observe the assembly of heteroporous structures. If we take the difference Δf in per particle free energy of the hexagon and stretched pore systems for each guest shape, the small-hexagon guests have $\Delta f^{sm-hex} \approx -1.45kT$. Δf for the square guests is less negative, $\Delta f^{sq} \approx -1.05kT$, showing that the squares have a lower thermodynamic driving force to form hexagon motifs. We also observe this difference in the HPMC simulations, which show small-hexagon-guest systems assembling more hexagon pores than in the square-guest systems (Fig. 2c,d). Despite a negative Δf for hexagon versus stretched hexagon pores in both systems (indicating thermodynamic preference for hexagon pores), it is small, on the order of thermal fluctuations, and self-assembly yields a heteroporous structure. The resulting heteroporeness means the shape of the $A_{f,guest}(\theta)$ curves in the different pore shapes determines the discreteness of the guest rotator phase, as discussed above.

4 Conclusions

We have shown that binary mixtures of hard, star-shaped host particles and convex polygonal guest particles can self-assemble into a variety of open, homoporous and heteroporous, HG structures. Notably, the host particles in this system can be synthesized without nanolithography. For example, “tripod” nanoplates, similar in shape to the star particles considered in this work, have been synthesized,⁴⁸ and are therefore a candidate for experimental realization of this HG-mediated self-assembly strategy. Additionally, all guest shapes (except for the shields) can be readily synthesized as nanoplates^{49–51}. These HG systems thereby provide a promising platform to assemble both homo- and heteroporous host crystals via a simple guest shape change. The rules for assembly and thermodynamic properties of these HG lattices are intuitive and guest-pore combinations can be designed via simple geometric and symmetry considerations, opening the door for the design of a new class of self-assembled nanoparticle superlattices.

Author Contributions

TD designed and performed the simulations and analyzed the data. All authors discussed the results and contributed to the writing of the manuscript. SCG directed the research.

Conflicts of interest

There are no conflicts to declare.

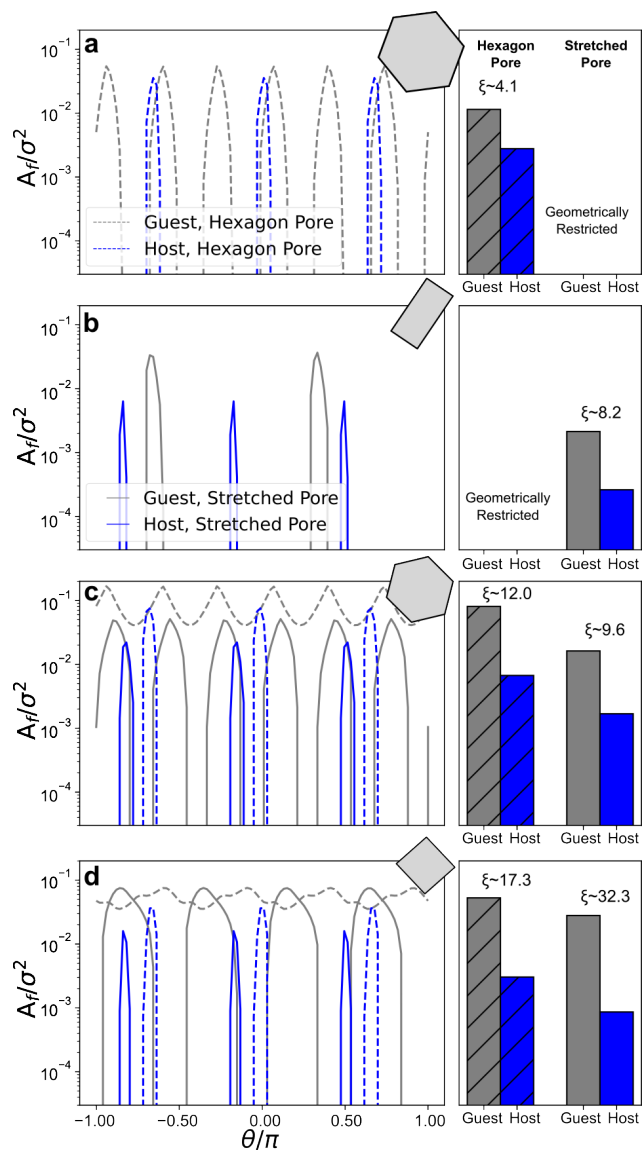


Fig. 5 Summary of free volume calculations, where each row corresponds to a guest shape; a: large hexagons; b: rectangles; c: small hexagons; and d: squares. The plots on the left of each row show the free volume A_f available to host (blue) and guest (gray) particles as a function of orientation θ in hexagon (dashed lines) and stretched pores (solid lines). The plots on the right show the average free volume \bar{A}_f for guest (gray bars) and host (blue bars) particles in hexagon (striped bars) and stretched (solid bars). ξ indicates the degree of entropy compartmentalization defined as the average free volume available to the guests relative to that of the hosts; higher values indicate more entropy compartmentalization.

Acknowledgements

This research was supported in part by the National Science Foundation, Division of Materials Research Award No. DMR 1808342 and by a grant from the Simons Foundation (256297, SCG). This research was also supported by a National Science foundation Graduate Research Fellowship to TD. This work used resources from the Extreme Science and Engineering Discovery Environment (XSEDE), which is supported by National Science Foundation grant number ACI-1548562; XSEDE Award DMR 140129.

Notes and references

- 1 P. F. Damasceno, M. Engel and S. C. Glotzer, *Science*, 2012, **337**, 453–457.
- 2 P. F. Damasceno, M. Engel and S. C. Glotzer, *ACS Nano*, 2012, **6**, 609–614.
- 3 A. T. Cadotte, J. Dshemuchadse, P. F. Damasceno, R. S. Newman and S. C. Glotzer, *Soft Matter*, 2016, **12**, 7073–7078.
- 4 R. Ni, A. P. Gantapara, J. d. Graaf, R. v. Roij and M. Dijkstra, *Soft Matter*, 2012, **8**, 8826–8834.
- 5 A. Castelli, J. de Graaf, M. Prato, L. Manna and M. P. Arciniegas, *ACS Nano*, 2016, **10**, 4345–4353.
- 6 P. K. Bommineni, M. Klement and M. Engel, *Physical Review Letters*, 2020, **124**, 218003.
- 7 E. S. Harper, G. van Anders and S. C. Glotzer, *Proceedings of the National Academy of Sciences*, 2019, **116**, 16703–16710.
- 8 L. Onsager, *Annals of the New York Academy of Sciences*, 1949, **51**, 627–659.
- 9 Y. Geng, G. van Anders, P. M. Dodd, J. Dshemuchadse and S. C. Glotzer, *Science Advances*, 2019, **5**, eaaw0514.
- 10 A. S. Karas, J. Dshemuchadse, G. van Anders and S. C. Glotzer, *Soft Matter*, 2019, **15**, 5380–5389.
- 11 G. van Anders, N. K. Ahmed, R. Smith, M. Engel and S. C. Glotzer, *ACS Nano*, 2014, **8**, 931–940.
- 12 R. K. Cersonsky, J. Dshemuchadse, J. Antonaglia, G. van Anders and S. C. Glotzer, *Physical Review Materials*, 2018, **2**, 125201.
- 13 J. F. Galisteo-Lopez, M. Ibisate, R. Sapienza, L. S. Froufe-Perez, A. Blanco and C. Lopez, *Advanced Materials*, 2011, **23**, 30–69.
- 14 A. T. Fafarman, S.-H. Hong, H. Caglayan, X. Ye, B. T. Diroll, T. Paik, N. Engheta, C. B. Murray and C. R. Kagan, *Nano Letters*, 2013, **13**, 350–357.
- 15 J. D. Joannopoulos, P. R. Villeneuve and S. Fan, *Nature*, 1997, **386**, 143–149.
- 16 W. Miller, C. W. Smith, D. S. Mackenzie and K. E. Evans, *Journal of Materials Science*, 2009, **44**, 5441–5451.
- 17 A. Love, *A treatise on the mathematical theory of elasticity*, 1892, vol. 1.
- 18 K. K. Saxena, R. Das and E. P. Calius, *Advanced Engineering Materials*, 2016, **18**, 1847–1870.
- 19 K. Sun, A. Souslov, X. Mao and T. C. Lubensky, *Proceedings of the National Academy of Sciences*, 2012, **109**, 12369–12374.
- 20 X. Mao and T. C. Lubensky, *Physical Review E*, 2011, **83**, 011111.
- 21 Q.-L. Lei, W. Zheng, F. Tang, X. Wan, R. Ni and Y.-q. Ma, *Physical Review Letters*, 2021, **127**, 018001.
- 22 G. Ernst, C. Broholm, G. R. Kowach and A. P. Ramirez, *Nature*, 1998, **396**, 147–149.
- 23 U. Vietze, O. Krauß, F. Laeri, G. Ihlein, F. Schüth, B. Limburg and M. Abraham, *Physical Review Letters*, 1998, **81**, 4628–4631.
- 24 N. Jiang, R. Shang, S. G. J. Heijman and L. C. Rietveld, *Water Research*, 2018, **144**, 145–161.
- 25 D. Ruthven, K. Loughlin and K. Holborow, *Chemical Engineering Science*, 1973, **28**, 701–709.
- 26 N. Pakalidou, J. Mu, A. J. Masters and C. Avendaño, *Molecular*

- Systems Design & Engineering*, 2020, **5**, 376–384.
- 27 N. Pakalidou, D. L. Cheung, A. J. Masters and C. Avendaño, *Soft Matter*, 2017, **13**, 8618–8624.
 - 28 A.-P. Hynninen, J. H. J. Thijssen, E. C. M. Vermolen, M. Dijkstra and A. van Blaaderen, *Nature Materials*, 2007, **6**, 202–205.
 - 29 P. Bartlett, R. H. Ottewill and P. N. Pusey, *Physical Review Letters*, 1992, **68**, 3801–3804.
 - 30 M. Eldridge, P. Madden, P. Pusey and P. Bartlett, *Molecular Physics*, 1995, **84**, 395–420.
 - 31 E. S. Harper, R. L. Marson, J. A. Anderson, G. van Anders and S. C. Glotzer, *Soft Matter*, 2015, **11**, 7250–7256.
 - 32 S. Lee, T. Vo and S. C. Glotzer, *Nature Chemistry*, 2023, 1–8.
 - 33 T. C. Moore, J. A. Anderson and S. C. Glotzer, *Soft Matter*, 2021, **17**, 2840–2848.
 - 34 J. A. Anderson, M. Eric Irrgang and S. C. Glotzer, *Computer Physics Communications*, 2016, **204**, 21–30.
 - 35 J. A. Anderson, J. Glaser and S. C. Glotzer, *Computational Materials Science*, 2020, **173**, 109363.
 - 36 W. Qi, J. de Graaf, F. Qiao, S. Marras, L. Manna and M. Dijkstra, *The Journal of Chemical Physics*, 2013, **138**, 154504.
 - 37 A. Haji-Akbari, M. Engel and S. C. Glotzer, *The Journal of Chemical Physics*, 2011, **135**, 194101.
 - 38 C. S. Adorf, P. M. Dodd, V. Ramasubramani and S. C. Glotzer, *Computational Materials Science*, 2018, **146**, 220–229.
 - 39 V. Ramasubramani, B. D. Dice, E. S. Harper, M. P. Spellings, J. A. Anderson and S. C. Glotzer, *Computer Physics Communications*, 2020, **254**, 107275.
 - 40 C. R. Harris, K. J. Millman, S. J. van der Walt, R. Gommers, P. Virtanen, D. Cournapeau, E. Wieser, J. Taylor, S. Berg, N. J. Smith, R. Kern, M. Picus, S. Hoyer, M. H. van Kerkwijk, M. Brett, A. Haldane, J. F. del Río, M. Wiebe, P. Peterson, P. Gérard-Marchant, K. Sheppard, T. Reddy, W. Weckesser, H. Abbasi, C. Gohlke and T. E. Oliphant, *Nature*, 2020, **585**, 357–362.
 - 41 J. D. Hunter, *Computing in Science Engineering*, 2007, **9**, 90–95.
 - 42 V. Ramasubramani, B. Dice, T. Dwyer and S. Glotzer, *Journal of Open Source Software*, 2021, **6**, 3098.
 - 43 A. Stukowski, *Modelling and Simulation in Materials Science and Engineering*, 2009, **18**, 015012.
 - 44 J. Towns, T. Cockerill, M. Dahan, I. Foster, K. Gaither, A. Grimshaw, V. Hazlewood, S. Lathrop, D. Lifka, G. D. Peterson, R. Roskies, J. R. Scott and N. Wilkins-Diehr, *Computing in Science Engineering*, 2014, **16**, 62–74.
 - 45 W. Shen, J. Antonaglia, J. A. Anderson, M. Engel, G. van Anders and S. C. Glotzer, *Soft Matter*, 2019, **15**, 2571–2579.
 - 46 J. A. Millan, D. Ortiz, G. van Anders and S. C. Glotzer, *ACS Nano*, 2014, **8**, 2918–2928.
 - 47 B. P. Prajwal and F. A. Escobedo, *Physical Review Materials*, 2021, **5**, 024003.
 - 48 T. Paik and C. B. Murray, *Nano Letters*, 2013, **13**, 2952–2956.
 - 49 Y. C. Cao, *Journal of the American Chemical Society*, 2004, **126**, 7456–7457.
 - 50 L. Li, J. Zhao, Y. Wang, Y. Li, D. Ma, Y. Zhao, S. Hou and X. Hao, *Journal of Solid State Chemistry*, 2011, **184**, 1661–1665.
 - 51 H. Hu, J. Zhou, Q. Kong and C. Li, *Particle & Particle Systems Characterization*, 2015, **32**, 796–808.